RESEARCH ARTICLE

Rhenium solubility and speciation in aqueous fluids at high temperature and pressure

Bjorn Mysen[1*] (ID)

Abstract

In order to characterize rhenium transport via infiltration of fluids in the Earth's interior, the solubility and solution mechanisms of ReO_2 in aqueous fluids were determined to 900 °C and about 1710 MPa by using an externally–heated hydrothermal diamond anvil cell. In order to shed light on how Re solubility and solution mechanisms in aqueous fluids can be affected by interaction of Re with other solutes, compositions ranged from the comparatively simple ReO_2–H_2O system to compositionally more complex Na_2O–ReO_2–SiO_2–H_2O fluids. Fluids in the ReO_2–SiO_2–H_2O, SiO_2–H_2O, Na_2O–SiO_2–H_2O, and Na_2O–ReO_2–H_2O systems also were examined. The presence of Na_2O enhances the ReO_2 solubility so that in Na_2O–ReO_2–H_2O fluids, for example, Re solubility is increased by a factor of 10–15 compared with the Re solubility in Na_2O-free ReO_2–H_2O fluids. The SiO_2 component in ReO_2–SiO_2–H_2O causes reduction of ReO_2 solubility compared with ReO_2–H_2O fluids. The ReO_2 solubility in the Na-bearing Na_2O–ReO_2–SiO_2–H_2O fluids is greater than that in fluids in both the ReO_2–H_2O and ReO_2–SiO_2–H_2O systems. Rhenium is dissolved in aqueous fluid as ReO_4-complexes with Re in fourfold coordination with oxygen. Some, or all, of the oxygen in these complexes is replaced by OH-groups depending on whether Na_2O also is present. It is proposed that during dehydration of hydrated subduction zone mineral assemblages in the upper mantle, the alkali/alkaline earth ratio of the source of the released aqueous fluid affects the extent to which Re (and other HFSE) can be transported into an overlying peridotite mantle wedge. The infiltration of such fluids will, in turn, affect the Re content (and Re/Os ratio) of magma formed by partial melting of this peridotite wedge.

Keywords Aqueous fluid, High pressure, Structure, Rhenium solubility, Spectroscopy, Rhenium solution mechanisms, Structure

1 Introduction

The rhenium distribution in the Earth's interior is heterogeneous perhaps because of Re transport by infiltrating aqueous fluids (D'Souza and Canil 2018). For example, significant Re enrichments in the mantle wedge overlying subducting plates near continental margins have been reported (Becker 2000; Sun et al. 2003; Tassara et al. 2018; Crossley et al. 2020). This enrichment could be the result of Re transfer from dehydrating slab materials to the overlying peridotite wedge during slab descent into the mantle. During partial melting of a peridotite wedge altered by the infiltrating fluids, its Re signature can be imparted on the partial melt. This signature could depend on temperature, pressure, redox conditions, bulk composition of the slab source of the fluid, and the fluid composition itself because those variables may affect the solubility of Re in the infiltrating fluid.

*Correspondence:
Bjorn Mysen
bmysen@carnegiescience.edu
[1] Carnegie Instn. Washington, 5241 Broad Branch Rd., Washington, D.C., NW 20015, USA

The solubility of an element in fluid can vary significantly depending on whether or not other solutes are present. For example, for a simple system such as Al_2O_3–H_2O, the alumina solubility under deep crustal and upper mantle conditions is on the order of tens of ppm (Becker et al. 1983; Ragnarsdóttir and Walther 1985; Tropper and Manning 2007). However, in the presence of, in particular, alkali metals such as Na^+ and K^+, the Al_2O_3 solubility increases by several orders of magnitude (Anderson and Burnham 1983; Pascal and Anderson 1989; Diakonov et al. 1996; Wohlers et al. 2011). Similar solubility behavior has been reported for nominally insoluble minor and trace elements such as Ti^{4+} and Zr^{4+}. In pure H_2O at deep crustal and upper mantle temperature and pressure conditions, the TiO_2 and ZrO_2 solubility is on the order of a few to a few tens of ppm (Audétat and Keppler 2005; Antignano and Manning 2008; Mysen 2012, 2015; Bernini et al. 2013; Louvel et al. 2013). However, with other solutes such as alkali metals, and perhaps SiO_2, under similar temperature and pressure conditions, both TiO_2 and ZrO_2 solubility increases by several orders of magnitude (Antignano and Manning 2008; Hayden and Manning 2011; Wilke et al. 2012, 2013; Mysen 2012, 2015, 2022). Rhenium may exhibit similar solution behavior, but relevant experimental data appear not to be available.

In order to characterize the influence of fluid transport on major, minor, and trace element concentrations in the Earth's interior, it is necessary to establish how their solubility in fluid and fractionation between fluid and condensed phases (magmatic liquid and mineral assemblages) depend on fluid composition, temperature, pressure, and, for some elements, redox conditions (see, for example, Pokrovski et al. 2013; Stefánsson et al. 2013, for reviews). It is also necessary to establish how interaction between other solutes affects solution mechanisms and solubility of elements of interest in the fluid (Diakonov et al. 1996; Azaroual et al. 1996; Wohlers et al. 2011; Manning 2018).

Whether, or the extent to which, interaction between rhenium and other solutes in fluids may take place, is not well known. However, in light of such effects on the solubility of other metals including geochemically similar elements (Bali et al. 2011, 2012; Ulrich and Mavrogenes 2008; Klein-BenDavid et al. 2011; Watenphul et al. 2014) and because of the importance of characterization of rhenium distribution in the Earth's interior (e.g., Tassara et al. 2018; Crossley et al. 2020), examination of possible effects of Re complexing with other solutes on Re solubility and Re solution mechanisms in high-temperature/-pressure H_2O-rich fluids relevant to upper mantle conditions is the principal objective of the present report.

2 Experimental methods

Examination of fluid-bearing samples comprised of ReO_2 and other oxides was conducted experimentally while the samples were at the desired temperatures and pressures. Experiments were carried out in this way because structure and solubility of oxide components in aqueous fluids at high temperature and pressure cannot be determined with precision by examination of the fluids after their quenching back to ambient temperature and pressure.

Characterization while at high temperature and pressure was accomplished by using externally heated, hydrothermal diamonds cells (HDAC) based on the design by Bassett et al. (1994). The optical access through the diamond windows in these diamond anvil cells allows for petrographic and spectroscopic examination of the sample while at the temperature and pressure of interest. In the present study, samples were characterized with optical examination and Raman spectroscopy.

Four different Re-containing mixtures (ReO_2–H_2O, ReO_2–SiO_2–H_2O, Na_2O–ReO_2–H_2O, and Na_2O–ReO_2–SiO_2–H_2O) were used as starting materials to assess effects of interactions among dissolved components such as Na_2O and SiO_2 on rhenium speciation and solubility in aqueous fluids. In addition, two starting compositions without ReO_2, but with SiO_2 (SiO_2–H_2O and Na_2O–SiO_2–H_2O), were employed to aid in the identification of spectroscopic features from Si–O bonding in species in (Si + Re)-bearing fluids.

The starting materials were comprised of double-distilled H_2O, H_2O with 1 molar NaOH, and spectroscopically pure crystalline ReO_2 and SiO_2. The Na- and Si-components were chosen as additional solutes because they have been demonstrated to cause pronounced solubility changes of components that are nearly insoluble in H_2O alone (Pascal and Anderson 1989; Hayden and Manning 2011; Wilke et al. 2012; Louvel et al. 2013).

The samples in the HDAC were contained in 125 μm thick Re gaskets with a central 500 μm-diameter sample containment hole between the two opposing diamonds with 1 mm culets. Sample temperatures were monitored with two K-type thermocouples touching both the upper and lower diamonds of the HDAC. Temperature variations within the cell, assessed with NaCl melting, which melts at 801.5 °C at ambient pressure, were 2–3 °C.

Pressure in the hydrothermal diamond anvil cell was generated by increasing the temperature, which causes increased pressure from the H_2O-rich fluid of the sample. This pressure is governed by the PVT properties of H_2O (Wagner and Pruss 2002), or, more precisely, from the oxide-saturated aqueous fluids. However, because the sample volume varies with temperature and pressure, pressure calculations from PVT properties yield

unreliable result. Moreover, the PVT properties of oxide-saturated fluids also are affected by such solutes (Mysen 2010; Wilke et al. 2013). Therefore, actual pressure was determined from the one-phonon Raman shift of synthetic ^{13}C diamond. This Raman shift depends on pressure and temperature (e.g., Schiferl et al. 1997).

Pressure determination from the one-phonon Raman shift of the ^{13}C diamond, placed within the fluid, was accomplished by using the pressure-/temperature-calibrated Raman shift (Mysen and Yamashita 2010). Carbon-13 diamond was used for this purpose to avoid interference of the Raman signal from the natural diamond anvils in the diamond anvil cell. The frequency difference between the one-phonon Raman shifts from natural diamond of the diamond anvils, which are nearly 100% carbon-12, and the synthetic carbon-13 diamond is about 80 cm^{-1} (Hanfland et al. 1985). The carbon-13 diamonds were synthesized with a CVD method where $^{13}CH_4$ gas was the source of carbon from which to grow diamonds (Liang et al. 2013).

Raman spectra were recorded with a JASCO™ micro-Raman spectrometer equipped with confocal optics, a single monochromator, a holographic notch filter and holographic gratings. The confocal optics reduce the focal depth of the laser beam used to excite the sample, which, in turn, diminishes the potential for interference with a sample signal from adjacent materials. Raman excitation was achieved by using the 490 nm line of a Coherent MX-Series solid state laser with ~40 mW laser power at the sample.

For pressure determination with the one-phonon shift of the ^{13}C diamond spectrum, 2400 grooves/mm grating density was employed to maximize accuracy of the spectrometer. This accuracy (± 1 cm^{-1}) was improved further by using emission lines from a Neon lamp as internal standard. A ± 0.1 cm^{-1} frequency uncertainty is attained with this design. This uncertainty translates to a ± 40 MPa precision of pressure measurements. The overall pressure uncertainty in the HDAC experiments, which also incorporates the uncertainty in the pressure/temperature calibration of the one-phonon Raman shift of the carbon-13 diamond from Mysen and Yamashita (2010), is ± 110 MPa.

Each of the starting compositions was subjected to nearly the same temperature sequence. However, even though the temperatures were similar, the pressure–temperature trajectories of these individual experimental series differed because the proportion of fluid and solids (crystalline ReO_2 and SiO_2) differed in each experiment so that the fluid volume and, therefore, the pressure exerted by this fluid, was different. It is not feasible to load the same proportions of fluid and solids in the sample hole of the Re gaskets because of the small sample volume in the diamond cell sample containment design (volume ~$15\cdot10^{-3}$ mm^3).

In each experimental temperature/pressure measurement series, the fluid + oxide sample was first brought to the highest planned temperature with its corresponding pressure and left there for about an hour prior to recording spectra while the sample remained at this temperature and pressure. Following measurements at a pressure/temperature condition, the next lowest temperature/pressure condition was reached with a 1 °C/s cooling rate. The 60-min dwell time at each temperature and pressure before spectroscopic measurements was considered sufficient to reach equilibrium with the present experimental configuration given that similar experimental duration has been shown sufficient to establish isotopic equilibrium between fluid and condensed phases at similar temperatures (Mysen 2015). Spectra of carbon-13 diamond were recorded at each temperature to determine the pressure.

3 Results and discussion

Crystalline ReO_2 and SiO_2 powders, together and individually, coexisting with aqueous fluid were present in the experiment (e. g., Fig. 1). The experiments were carried out in the 550–900 °C and about 150–1710 MPa temperature and pressure ranges, respectively (Fig. 2). The temperature–pressure relationships in Fig. 2 must be kept in mind, therefore, when reference is made to temperature of an experiment in this report.

3.1 Raman spectroscopy and solution mechanisms in fluid

Raman spectra were recorded in the 300–1200 cm^{-1} range (low-frequency range) where Raman signals from vibrations of Re–O and Si–O bonds can be detected. Raman signals in this frequency range were used, therefore, to examine structural features of oxide components dissolved in the aqueous fluid.

Spectra recorded in the 3000–4000 cm^{-1} range (high-frequency range) comprise signals assigned to stretch vibrations from OH-groups. These OH-groups can be a part of molecular H_2O or as OH-groups that form bonding with metal cations dissolved in aqueous fluid.

3.1.1 Low-frequency range (300–1200 cm^{-1})

The Raman spectra of ReO_2–H_2O fluids in the 300–1200 cm^{-1} frequency range characteristically are comprised of three bands near 320 cm^{-1}, 920 cm^{-1} and 960 cm^{-1}, respectively (Fig. 3A). The same three bands were observed in spectra of Na_2O–ReO_2–H_2O fluid. In addition, in this latter system, a fourth band was observed near 1040 cm^{-1} (Fig. 3B).
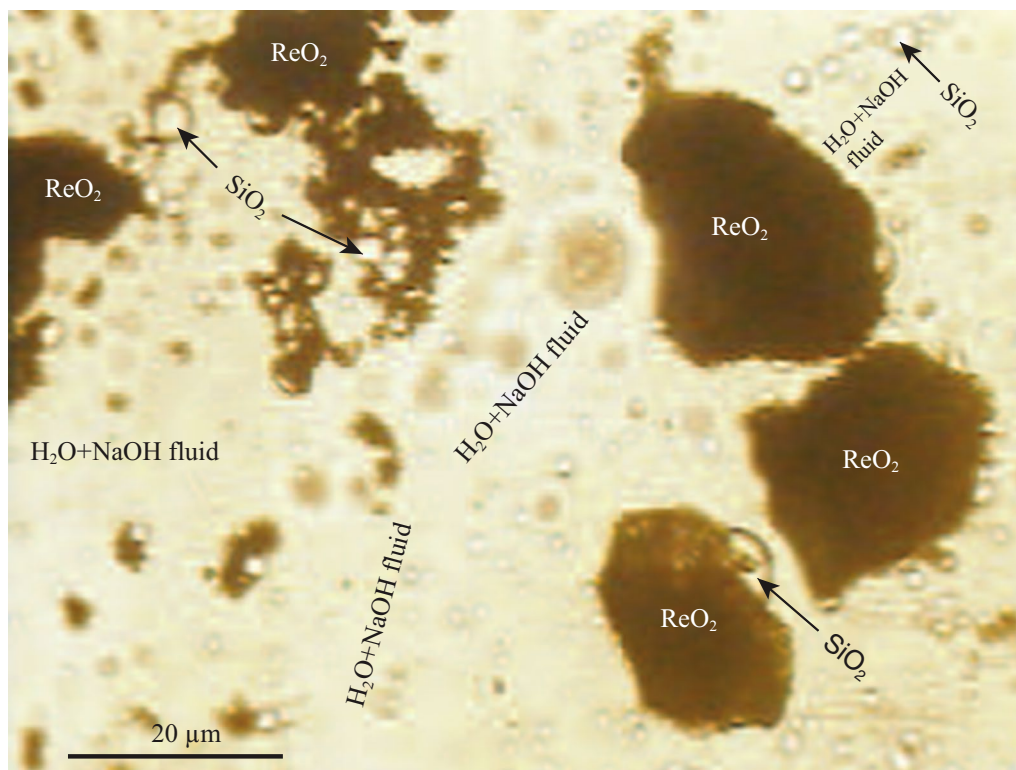
Fig. 1 Photomicrograph Na_2O–ReO_2–SiO_2–H_2O fluid and solid SiO_2 and ReO_2 while in the hydrothermal diamond anvil cell at 550 °C and 250 MPa. Individual phases are identified on photo
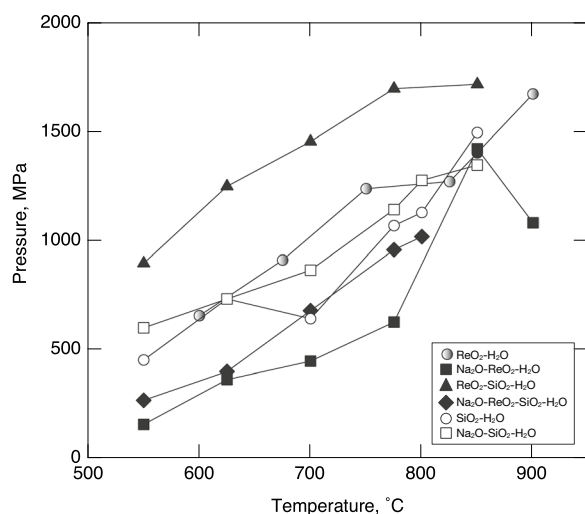

Fig. 2 Pressure–temperature trajectories of the 6 different experimental series conducted in this project. Individual systems are identified in the caption on the figure

The 320, 920, 960 cm^{-1} bands in the spectrum of ReO_2–H_2O fluid occur at frequencies similar to those from Re−O vibrations in isolated ReO_4 groups such as existing in crystalline ReO_2 in which Re^{4+} is in fourfold coordination with oxygen and also from calculated spectra of isolated ReO_4 groups (Busey and Keller 1964; Weinstock et al. 1973). It seems reasonably to conclude, therefore, that in fluids in the ReO_2–H_2O system, dissolved Re^{4+} also occupies fourfold coordination with oxygen perhaps forming isolated rhenate groups (ReO_4).

The rhenium solution mechanism in aqueous fluid in the simple ReO_2–H_2O system, may be described, therefore, with the expression:

$$ReO_2 + 2H_2O \Leftrightarrow Re(OH)_4, \tag{1}$$
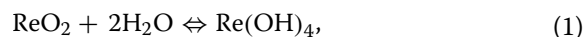
with the $Re(OH)_4$ structure schematically illustrated in Fig. 4A.

The Raman band near 1040 cm^{-1} in the spectra of Na_2O–ReO_2–H_2O fluid might reflect Re−O bonding in structural entities more polymerized than isolated ReO_4 groups (i.e., containing Re−O−Re bridges). This suggestion is based on analogy with the Si−O vibrations of bridging oxygen in silicate melts and in silicate-saturated aqueous fluid at sufficiently high temperature and pressure to stability polymerized silica complexes (Virgo et al. 1980; Zotov and Keppler 2002; Mysen 2010). In such silicate complexes, Si−O symmetric stretch vibrations also result in a broad Raman band near 1040–1060 cm^{-1} (Furukawa et al. 1981; Lasaga 1982).
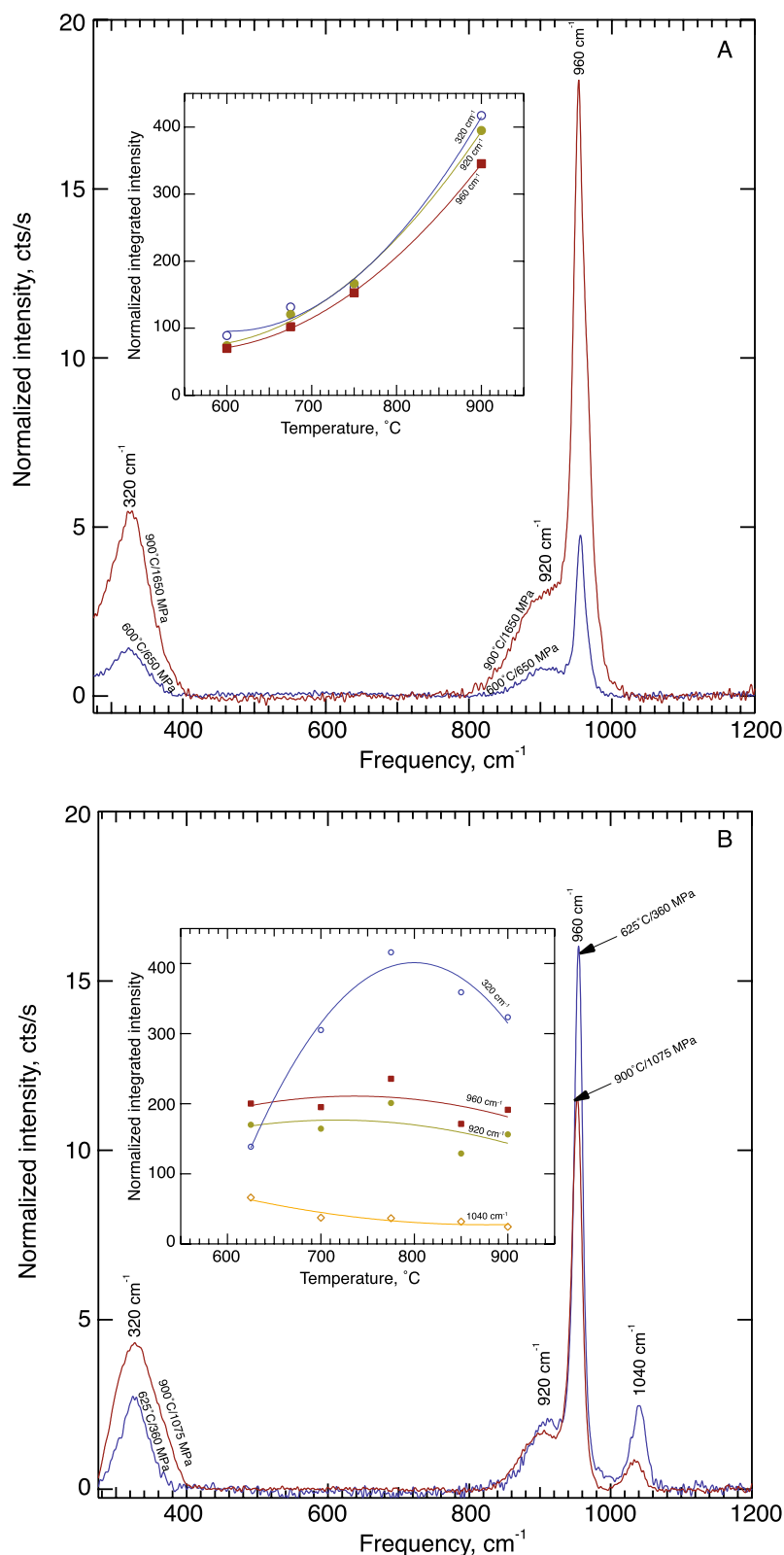
Fig. 3 Examples of Raman spectra in the 300–1200 cm^{-1} frequency range of fluids from systems without SiO$_2$. **A** ReO$_2$–H$_2$O and **B** Na$_2$O–ReO$_2$–H$_2$O at the temperatures and pressures indicated on the individual spectra. Inserts show the temperature evolution of the individual Raman bands. Pressures corresponding to each temperature can be read off Fig. 2. In this and subsequent figures, the Raman intensities are normalized to the same Raman setup parameters (acquisition time and slit width)
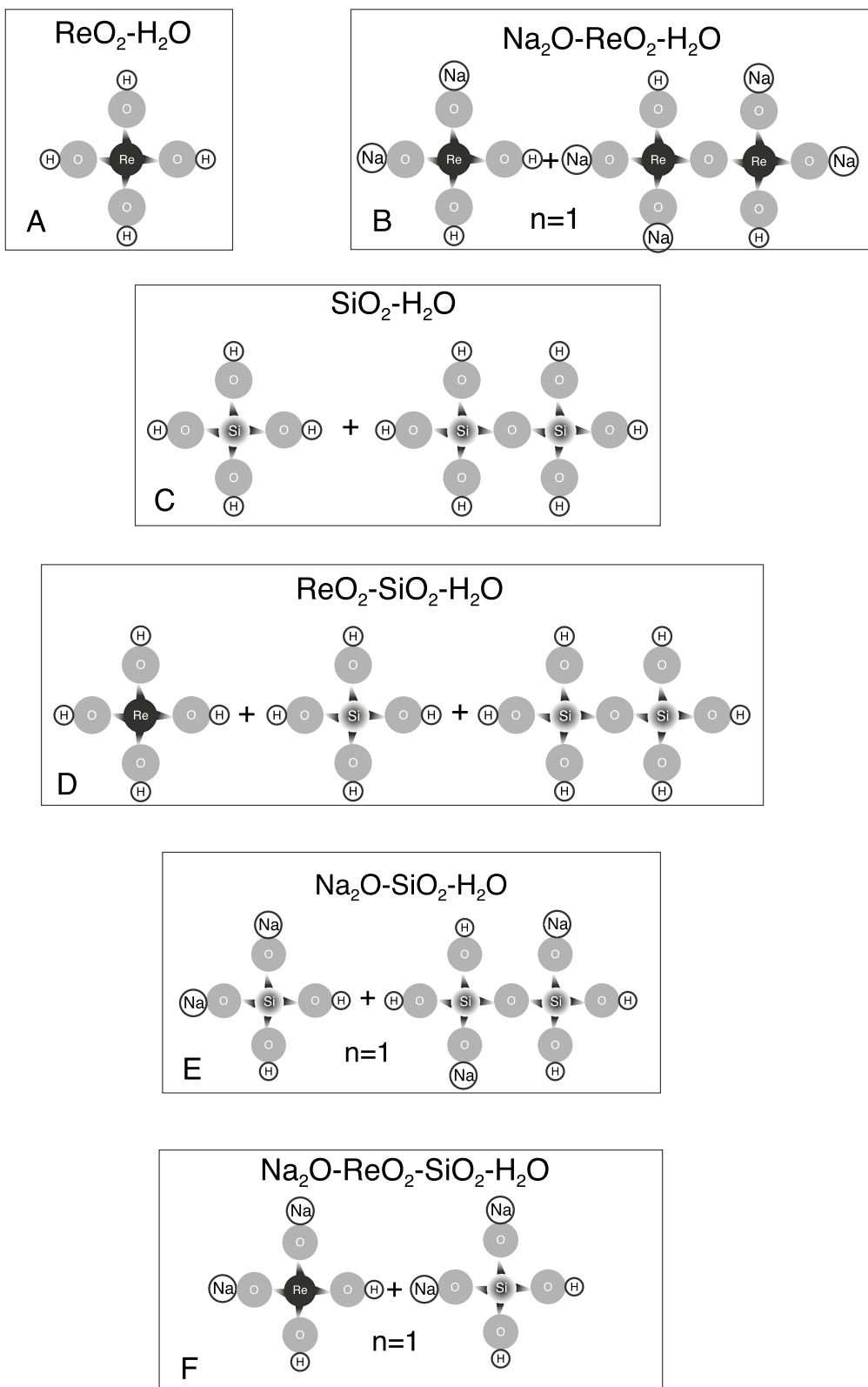
Fig. 4 Schematic representations of solution mechanisms in the fluids for systems as indicated on individual structures

Although details of the structure of polymerized rhenate groups is not clear from the experimental data, by using relationships between SiO_2 concentration and silicate polymerization in aqueous fluid and silicate melts as a guide (Mysen et al. 1982a, 2013), a pyrorhenate complex (Re_2O_7) seems most likely structural complex containing bridging oxygen. The solution mechanism of ReO_2 in $Na_2O–ReO_2–H_2O$ fluids may then be described as follows:

$$3ReO_2 + 2nH_2O + (5 − n)Na_2O$$
$$⇔ Na_{4−n}ReO_{4−2n}(OH)_{2n} \qquad (2)$$
$$+ Na_{6−2n}Re_2O_{7−2n}(OH)_{2n}.$$
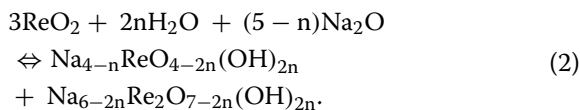
In Eq. (2), the value of n defines distribution of H^+ and Na^+ bonded to nonbridging oxygen in the ReO_4 and Re_2O_7 groups such as in Eq. (2) and illustrated schematically in Fig. 4B. From this information, the OH/Na abundance ratio in the orthorhenate groups ($Na_{4−n}ReO_{4−2n}(OH)_{2n}$) will always by greater than in the pyrorhenate group ($Na_{6−2n}Re_2O_{7−2n}(OH)_{2n}$) because the oxygen bridge between the two ReO_4 groups in the pyrorhenate complex is not bonded to either H^+ or Na^+ (e.g., Fig. 4B). We also note that the relationships in Eq. (2) and Fig. 4B do not consider possible complexes in the fluids that include Na–OH bonding. In analogy with the structural interpretation of ^1H and ^{29}Si MAS NMR spectra of hydrous Na-silicate melts in which isolated NaOH groups were found to be common (Cody et al. 2005), NaOH-type complexes probably also exist in the Re-bearing fluids.

In the spectra of $ReO_2–H_2O$ fluid, there is an approximately fourfold increase in integrated area of each of the three low-frequency bands with increasing temperature and pressure (from 600 °C/~600 MPa to 900 °C/~1700 MPa; see insert in Fig. 3A). If the Raman cross sections for these vibrations do not change with concentration and no other structural changes take place in the neighborhood of the Re–O bonds of interest, this observed intensity increase would correspond to a fourfold Re concentration increase in the fluids in this temperature and pressure range. Such a conclusion has been reported for sulfur species in aqueous fluids, for example (Schmidt and Seward 2017).

However, in the spectra of $Na_2O–ReO_2–H_2O$ fluids, the intensity of the three highest-frequency bands (920, 960, and 1040 cm^{-1}) all decrease with increasing temperature and pressure, whereas the lower-frequency 320 cm^{-1} band intensity appears to pass through a maximum at intermediate temperature and pressure (insert in Fig. 3B). Additional structural complexity likely exists here as evidenced by the 1040 cm^{-1} band. As discussed above, this band probably reflects the presence of Re–O–Re bridges

in the Re-complexes in these fluids. Under such circumstances, the intensity relations are not simply a function of the intensity of the Raman bands assigned to Re–O vibrations in other Re-bearing structural complexes in the fluid.

Raman spectra of fluid in systems that include both ReO_2 and SiO_2 ($ReO_2–SiO_2–H_2O$ and $Na_2O–ReO_2–SiO_2–H_2O$) are compared with the low-frequency spectra of ReO_2-free equivalent systems ($SiO_2–H_2O$ and $Na_2O–SiO_2–H_2O$) in Fig. 5. The spectra of $ReO_2–SiO_2–H_2O$ fluids (Fig. 5A) include the same bands as those in fluid spectra from $ReO_2–H_2O$ (320, 920, and 960 cm^{-1} bands; see also Fig. 3A). These three Raman bands are assigned to the same Re–O vibrations with Re in fourfold coordination with oxygen in the fluid (Re–O vibrations in ReO_4 groups).

The spectra of $ReO_2–SiO_2–H_2O$ fluid recorded at the highest temperatures and pressures examined contain two or three additional bands near 470, 650, and 780 cm^{-1} (Figs. 3A and 5A). These bands were not observed in the $ReO_2–H_2O$ fluid spectra. The 650 and 780 cm^{-1} bands also are evident in the spectra of $SiO_2–H_2O$ fluid (Fig. 5B). In the spectra of $SiO_2–H_2O$ fluids, there is also a weak band near 900 cm^{-1}. In spectra of both Re-bearing (Fig. 5A, C) and Re-free (Fig. 5B, D) fluids with SiO_2, the integrated Raman intensities of the latter bands grow with increasing temperature and pressure (Fig. 6). Their intensities in the spectra of Re-free $SiO_2–H_2O$ fluid exceed those in the spectra of $ReO_2–SiO_2–H_2O$ fluid (Fig. 6).

The 650, 780, and 900 cm^{-1} Raman bands in the spectra of $SiO_2–H_2O$ and $ReO_2–SiO_2–H_2O$ fluid are assigned to Si–O vibrations in silicate-bearing fluid species. In other structural studies of silicate speciation in $SiO_2–H_2O$ fluids at high temperature and pressure, the 780 cm^{-1} band has been assigned to Si–O stretch vibrations in isolated SiO_4 tetrahedra with H^+ attached to oxygen in the corners of those tetrahedra (Zotov and Keppler 2000; Mysen 2010, 2009). In the $SiO_2–H_2O$ fluids, there are two additional bands, near 650 and 900 cm^{-1}, respectively, as well as another band near 1040 cm^{-1} (Fig. 5D). The 650 cm^{-1} is assigned to Si–O–Si bending vibrations in polymerized silicate structures (Zotov and Keppler 2002), and the 1040 cm^{-1} band to Si–O stretch vibrations of bridging oxygen bonds (Furukawa et al. 1981; Lasaga 1982; Mysen et al. 1982a). The existence of those two bands do not define the number of oxygen bridges in this silicate structure, and merely the existence of bridging oxygens, which exist in all polymerized silicate structures. However, the 900 cm^{-1} band most likely should be assigned to Si–O stretching of a nonbridging Si–O bond in pyrosilicate (Si_2O_7) structure in silicate melts and silicate-saturated
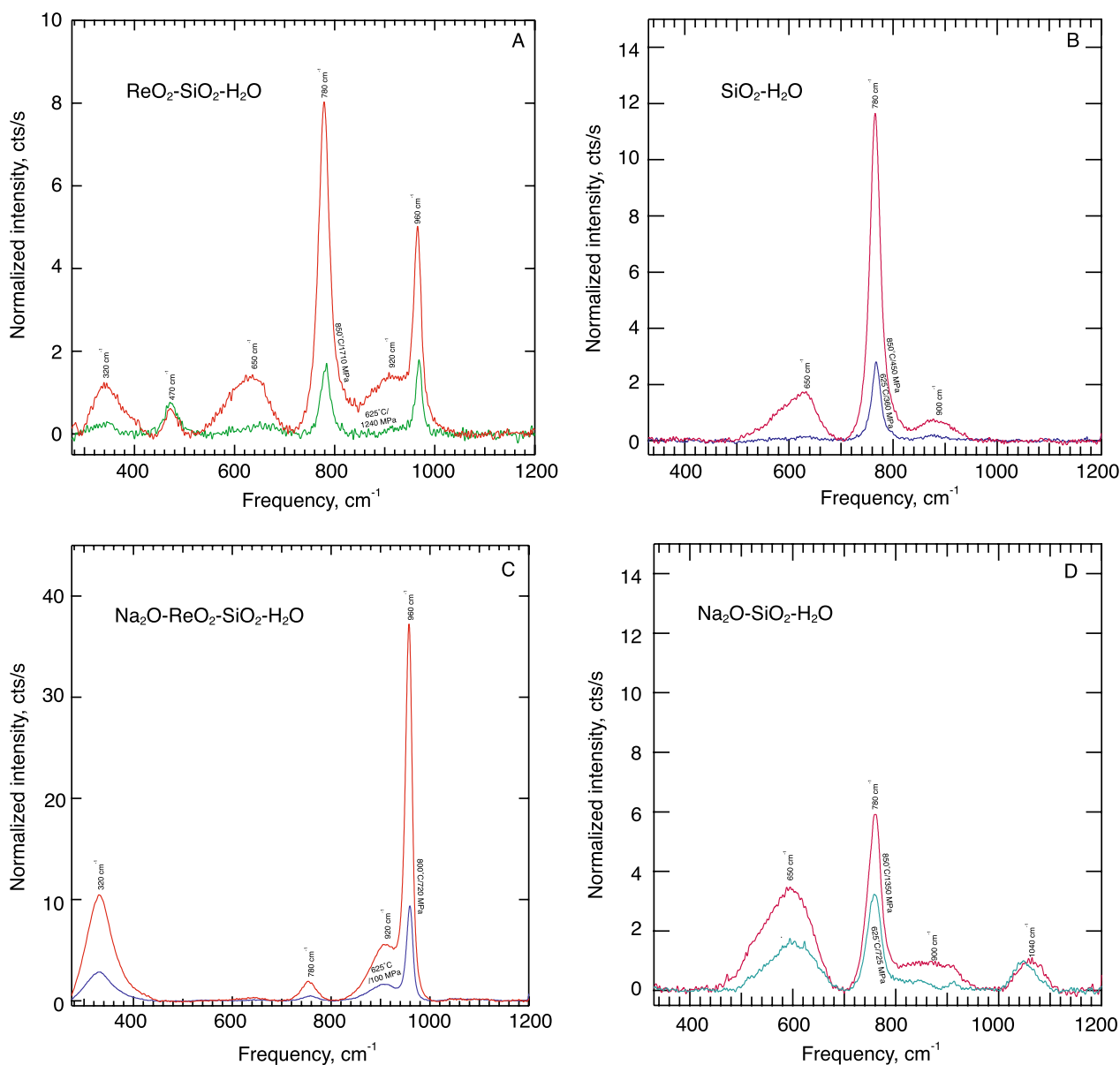
Fig. 5 Examples of Raman spectra of fluids in the 300–1200 cm^{-1} frequency range from systems that contain SiO$_2$ in addition to ReO$_2$. **A** Fluid spectra from the ReO$_2$–SiO$_2$–H$_2$O. **B** Fluid spectra from the SiO$_2$–H$_2$O. **C** Fluid spectra from the Na$_2$O–ReO$_2$–SiO$_2$–H$_2$O. **D** Fluid spectra from the Na$_2$O–SiO$_2$–H$_2$O. Raman intensities are normalized to the same Raman setup parameters (acquisition time and slit width)

aqueous fluids (Lasaga 1982; Seifert et al. 1982; Mysen 2009). This assignment also is consistent with the assignments of the 650 and 1040 cm^{-1} bands.

The simplest solution mechanism of SiO$_2$ in the SiO$_2$–H$_2$O fluids under the conditions of the present experiments can be described with the equation;

$$3SiO_2 + 5H_2O \Leftrightarrow Si(OH)_4 + Si_2O(OH)_6. \qquad (3)$$
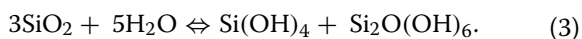
In the SiO$_2$–H$_2$O fluids, all the terminal oxygens in the SiO$_4$ groups have been replaced by OH groups. In the Si$_2$O$_7$ groups, all six terminal oxygens (nonbridging oxygens) have been replaced by OH groups. There is no H$^+$ bonded to the single bridging oxygen model in this model (see also Fig. 4C). These silicate structures are, therefore, analogous to the rhenate structures in ReO$_2$–H$_2$O, ReO$_2$–SiO$_2$–H$_2$O, and Na$_2$O–ReO$_2$–SiO$_2$–H$_2$O fluids in which
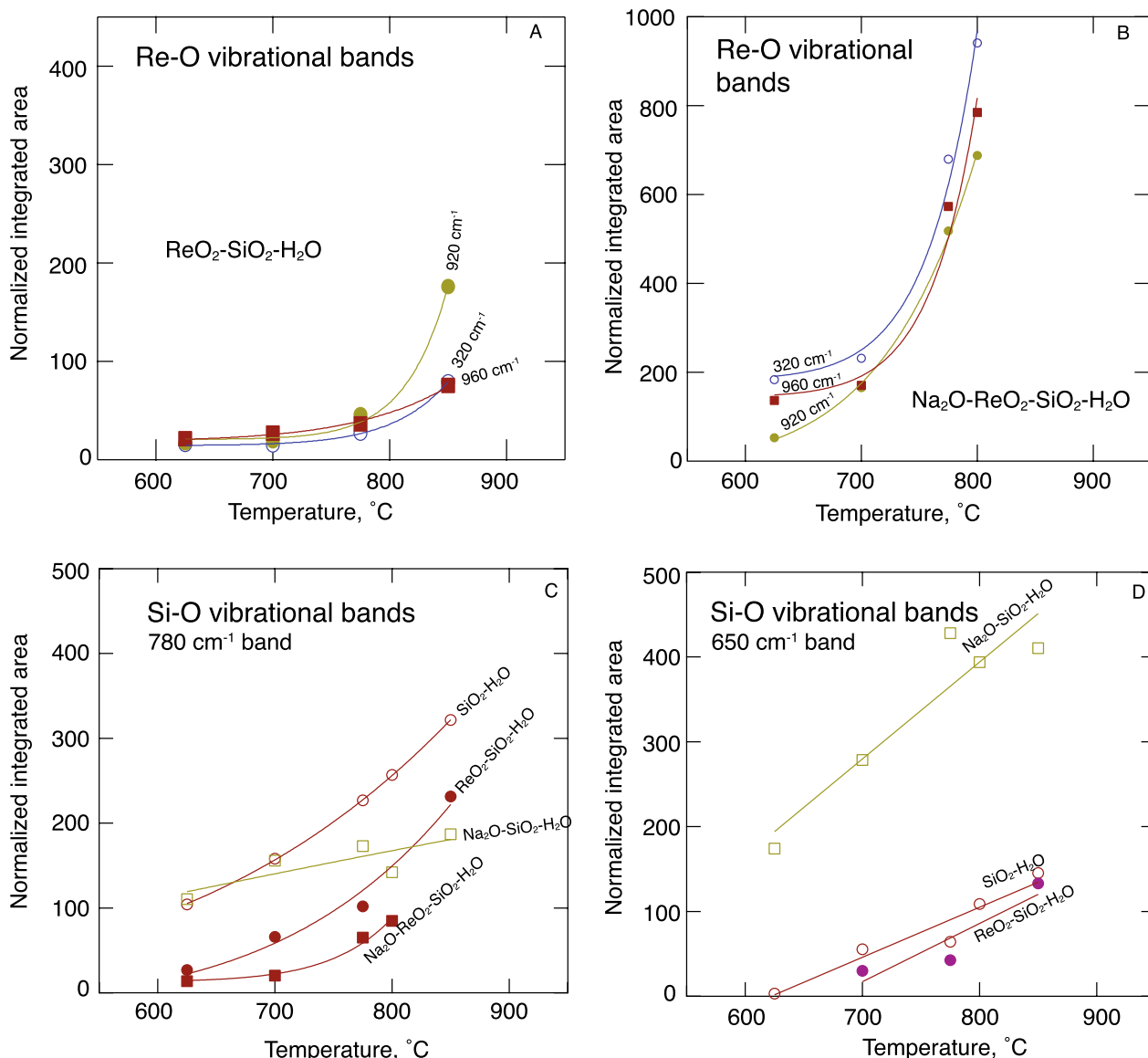
Fig. 6 Temperature evolution of integrated intensity Raman bands assigned to Re–O and Si–O vibrations in spectra of fluids as indicated on each curve. Pressures corresponding to each temperature can be read off Fig. 2. Raman intensities are normalized to the same Raman setup parameters (acquisition time and slit width). **A** Intensity evolution with temperature (and pressure) of bands assigned to Re–O vibrations in fluid from the ReO_2–SiO_2–H_2O. **B** Intensity evolution with temperature (and pressure) of bands assigned to Re–O vibrations in fluid from the Na_2O–ReO_2–SiO_2–H_2O. **C** Temperature evolution of intensity of Si–O stretch vibrations from isolated SiO_4 tetrahedra (780 cm^{-1} band) in fluids in systems that contain SiO_2. **D** Temperature evolution of intensity of Si–O–Si bend vibrations from polymerized SiO_4 tetrahedra (650 cm^{-1} band) in fluids in systems that contain SiO_2

Re^{4+}, instead of Si^{4+}, occupies the central position in the oxygen tetrahedra (compared Fig. 4B, C).

Silicate species in Na_2O–SiO_2–H_2O also include Si_2O_7 groups. In this latter system, the solution mechanism of silica, not including possible NaOH complexes, can be written as;

$$3SiO_2 + 2nNa_2O + (4-n)H_2O$$
$$\Leftrightarrow Na_{2n}SiO_{4-2n}(OH)_{4-2n}$$
$$+ Na_{2n}Si_2O_{5-2n}(OH)_{6-2n}, \tag{4}$$
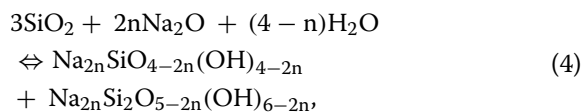
with the structure of the silicate species illustrated in Fig. 4E. Here, as in expression (2), both H^+ and Na^+ form bonding with terminal oxygen in the tetrahedra. Their proportion is governed by the value of *n*.

The Raman band near 650 cm^{-1} in the spectra of fluids in the ReO_2–SiO_2–H_2O system at the highest temperatures and pressures and in the spectra SiO_2–H_2O fluids at all temperatures and pressures, remains assigned to –O–bending vibrations. This means that the 650 cm^{-1} band in the spectra of ReO_2–SiO_2–H_2O fluids implies that some of the SiO_4 tetrahedra are more polymerized than an isolated SiO_4 tetrahedron. However, whether this bridging oxygen is from Re–O–Re, Re–O–Si, or Si–O–Si bridges cannot be determined from the Raman spectra. In the sketch in Fig. 4D, this feature in ReO_2–SiO_2–H_2O fluid is assumed to be Si–O–Si bridges resembling the structural features of SiO_2–H_2O fluids.

Because an intense 780 cm^{-1} band remains in the ReO_2–SiO_2–H_2O fluid spectra, isolated SiO_4 groups coexist with the more polymerized complexes in those fluids. The 900 cm^{-1} band in the spectra of high temperature and pressure ReO_2–SiO_2–H_2O fluids and in all the fluids from the SiO_2–H_2O system is assigned to Si–O stretch vibrations this polymerized silicate complex. This assignment is consistent with the assignment of the 650 cm^{-1} band because the 900 cm^{-1} together with that near 650 cm^{-1} is considered typical whenever Si_2O_7 entities (with one Si–O–Si bridge per Si) exist in the structure (Furukawa et al. 1981).

Rhenium is considerably heavier than Si. So, if we assume that the 900 cm^{-1} should be assigned to Re–O stretch vibrations in hypothetical Re_2O_7 or $ReSiO_7$ complexes, it is likely, that the frequency of Re–O stretch vibrations in such complexes would be at frequencies quite different, and likely lower much lower, than that of the Si–O stretch vibrations in an Si_2O_7 complex (Brawer and White 1975). It is concluded, therefore, that most likely the polymerized species in ReO_2–SiO_2–H_2O fluid is Si_2O_7.

From this structural interpretation of the ReO_2–SiO_2–H_2O spectra, the $ReO_2 + SiO_2$ solution mechanism in aqueous can be formulated with an expression such as:

$$ReO_2 + 3SiO_2 + 7H_2O$$
$$\Leftrightarrow Re(OH)_4 + Si(OH)_4 + Si_2O(OH)_6. \tag{5}$$
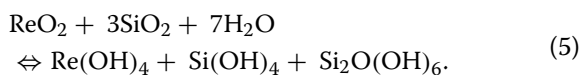
Schematic structure of coexisting silicate and rhenate complexes in the ReO_2–SiO_2–H_2O fluids are illustrated in Fig. 4D.

In SiO_2-bearing systems that also include Na_2O such as in the system Na_2O–ReO_2–SiO_2–H_2O, the spectra of their fluid comprise the same three bands as in the spectra of fluids in the Na_2O–ReO_2–H_2O. These bands were assigned to Re–O vibrations in ReO_4 groups (Figs. 3B

and 5C). There is no evidence for polymerized rhenate complexes in the Na_2O–ReO_2–H_2O fluids. In addition, in the Na_2O–ReO_2–SiO_2–H_2O fluid spectra, there is a weak band near 780 cm^{-1}. This band becomes more intense with increasing temperature and pressure (Figs. 5C and 6C). As in fluid spectra of other SiO_2-bearing systems, this band is assigned to Si–O stretch vibrations in isolated SiO_4 groups. However, none of the other bands assigned to Si–O stretch vibrations of silicate species such as in the spectra of the Na_2O-free ReO_2–SiO_2–H_2O fluids and ReO_2-free Na_2O–SiO_2–H_2O fluids were observed in the Na_2O–ReO_2–SiO_2–H_2O fluid spectra (Fig. 5). The silicate species in Na_2O–ReO_2–SiO_2–H_2O fluids is, therefore, only isolated SiO_4 tetrahedra where both H^+ and Na^+ form bonding with the terminal oxygen in this species.

The complete solution mechanism of rhenate and silicate in Na_2O–ReO_2–SiO_2–H_2O fluids can then be written as:

$$ReO_2 + SiO_2 + 2nH_2O + (4-2n)Na_2O$$
$$\Leftrightarrow Na_{4-2n}ReO_2(OH)_{2n} + Na_{4-2n}SiO_2(OH)_{2n}, \tag{6}$$
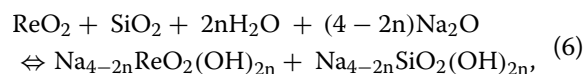
as also illustrated in the structural schematic in Fig. 4F.

3.1.2 High-frequency range (3000–4000 cm^{-1})

The high-frequency range of the Raman spectra of the aqueous fluids, between 3000 and 4000 cm^{-1}, comprises Raman bands assigned to O–H stretch vibrations from H_2O molecules and from OH-groups bonded to cations such as Si^{4+} and alkali metals, for example (Walrafen et al. 1986; Mysen and Virgo 1986; Le Losq et al. 2011). Bonding of OH-groups to rhenium cations to form Re–OH bonds also result in O–H stretch vibrations that give rise to Raman bands in this frequency range. This Raman intensity envelope, with peak maximum typically between 3550 and 3600 cm^{-1}, will be referred to as the 3600 cm^{-1} envelope.

The exact frequency or frequencies of Raman bands assigned to O–H vibrations in OH groups bonded to various metal cations depends somewhat on the electronic properties of the metal cation because electronic properties of the metal cation(s) will affect the strength, and, therefore, the frequency of O–H vibrations of the O–H bonds. For example, the frequency decreases as the metal cation becomes more electropositive (Mysen and Virgo 1986). Hydrogen bonding also will cause a frequency change (Walrafen et al. 1988, 1999; Frantz et al. 1993; Le Losq et al. 2015).

Quantitative evaluation of various possible OH-environments based on interpretation of the 3600 cm^{-1} envelope alone can be challenging, however, because of the often small frequency differences between of individual Raman bands of different OH stretch vibrations in the
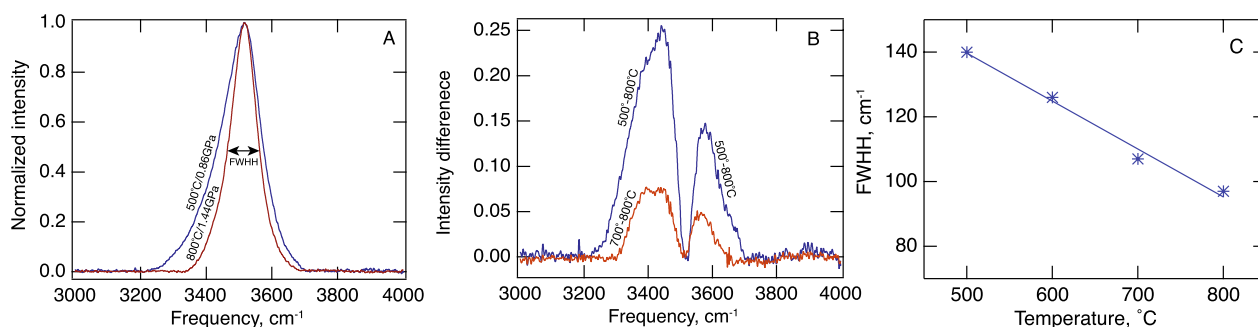
Fig. 7 Examples of Raman spectra of pure H_2O in the high-frequency range (3000–4000 cm^{-1}) at temperatures and pressures indicated on each spectrum. Spectra are normalized to the same acquisition time and slit width and then normalized to the maximum intensity within each spectrum, **A** 3600 cm^{-1} envelope at temperature/pressure conditions indicated on each spectrum. Intensities are normalized to the highest intensity point in each spectrum. **B** Difference spectra relative to 800 °C/1.44 GPa spectrum as indicated by temperature. **C** Evolution of full width at half height as a function of temperature (and pressure—see Fig. 2)

3600 cm^{-1} envelope. Temperature and to some degree, pressure, also affect the topology and frequency of the 3600 cm^{-1} envelope at least in part because the extent of hydrogen bonding is sensitive to temperature and pressure (Walrafen et al. 1988; Frantz et al. 1993; Kawamoto et al. 2004; Hoffmann and Conradi 1997; Sahle et al. 2013). Hydrogen bonding does, however, diminish rapidly with increasing temperature (Walrafen et al. 1988; Frantz et al. 1993; Foustoukos and Mysen 2012). Signals from hydrogen bonding typically cannot be detected at temperature above about 600–650 °C (Foustoukos and Mysen 2012). Effects of composition on the 3600 cm^{-1} envelope topology are not likely, therefore, to be significantly affected by effects of hydrogen bonding because for the most part experiments were conducted and above this temperature.

The high-frequency envelope in the temperature and pressure range of the present experiments (550–900 °C and about 380–1710 MPa) has a single maximum between 3500 and 3600 cm^{-1}. This envelope is slightly asymmetric to its low-frequency side of the ~3600 cm^{-1} intensity maximum (Figs. 7 and 8). This asymmetry may be because of different metal-OH bonds, hydrogen bonding, or both. The asymmetry also can be observed in spectra of pure H_2O (Fig. 7A, B), which also illustrate how the abundance of hydrogen bonding decreases with increasing temperature (Frantz et al. 1993; Hoffmann and Conradi 1997; Foustoukos and Mysen 2012). This abundance evolution is reflected in decreasing intensity of O−H vibrations on the low-frequency side of the O−H envelope in the high-temperature spectra of pure H_2O (Walrafen et al. 1988, 1999; Frantz et al. 1993).

Information on how the high-frequency spectra from Re- and Si-bearing fluid systems respond to temperature and pressure variations was extracted from difference spectra where Raman bands from lower temperature and

pressure were subtracted from those recorded at higher temperature and pressure. These spectra were normalized to the same Raman measurement conditions before subtraction.

Difference spectra for pure H_2O are illustrated in Fig. 7B. The sharp intensity dip near 3550 cm^{-1} in these spectra as well as in those from fluids from the other system reflects the fact that the peak maxima of these envelopes shift to lower frequencies with increasing temperature. Therefore, when subtracting a higher-from a lower-temperature spectrum a negative dip will occur near the intensity maximum of the lower-temperature spectrum.

The latter complication aside, the intensity on the low-frequency side of the high-frequency envelope from pure H_2O becomes less pronounced the higher the temperature, features that are similar to those originally reported by Walrafen et al. (1988) (Fig. 7B). This spectral evolution also is the primary cause of the decreased full width at half height (FWHH) of this envelope as the temperature is increased (Fig. 7C). This decrease reflects decreasing abundance of hydrogen bonding.

The spectral topologies of the high-frequency envelope from fluids in all systems resemble one another (Fig. 8). The spectra become narrower with increasing temperature (Fig. Fig. 8E, J, M, P). There are, however, differences in detail depending on the specific system considered because the rate of change of FWHH with temperature, $\partial FWHH/\partial T$, differs somewhat in the spectra of the various systems (Fig. 8P, Q). This FWHH change with temperature is emphasized in the difference spectra (Fig. 8B, D, G, I, L, O).

The FWHH of spectra of fluids from the Na_2O–ReO_2–H_2O system is greater than that in the fluid spectra from the Na-free, ReO_2–H_2O system (Fig. 8A, E, F, J; see also summary in Fig. 8P). Moreover, the $\partial FWHH/\partial T$ of

spectra in the Na_2O–ReO_2–H_2O system exceeds that of the compositionally simpler and Na-free ReO_2–H_2O system spectra (Fig. 8Q). One might infer that these differences reflect some effect on the OH bond strength of dissolved rhenate complexes when Na_2O is added to the ReO_2–H_2O system.

To create Re-OH bonding in Na_2O–ReO_2–H_2O fluids, one or more terminal oxygen in the ReO_4 tetrahedra is replaced with one or more OH groups and one or more ONa groups. Details of how Na-OH complexes may be linked to rhenate and/or rhenate/silicate structures in the aqueous fluids cannot be inferred from existing information. The Na^+ might form isolated NaOH groups analogous to the NaOH groups detected from NMR spectra of hydrous Na_2O–SiO_2 melts (Cody et al. 2005). However, more complex structures involving, for example, Na^+

linked to nonbridging oxygen in ReO_4 groups but also comprising Na–OH bonds, might also be involved.

The latter differences resemble those between the Re-free SiO_2–H_2O and Na_2O–SiO_2–H_2O high-frequency spectra (Fig. 8C, D, F, H, I, J). The structural interpretation of those differences spectra likely reflects effects of different O–H bond strength depending on the extent to which the OH-group forms bonding with Si^{4+} and Na^+. In the SiO_2–H_2O fluids, there can be only Si–OH bonding. The wider 3600 cm^{-1} envelope from Na_2O–SiO_2–H_2O fluid compared with the spectra of SiO_2–H_2O fluid is because there is some Na–OH bonding in the Na_2O–SiO_2–H_2O fluid. The O–H stretch vibrations from the OH-groups in Na-OH bonds result in Raman bands on the low-frequency side of the 3600 cm^{-1} envelope (Mysen and Virgo 1986; Mysen 2018).
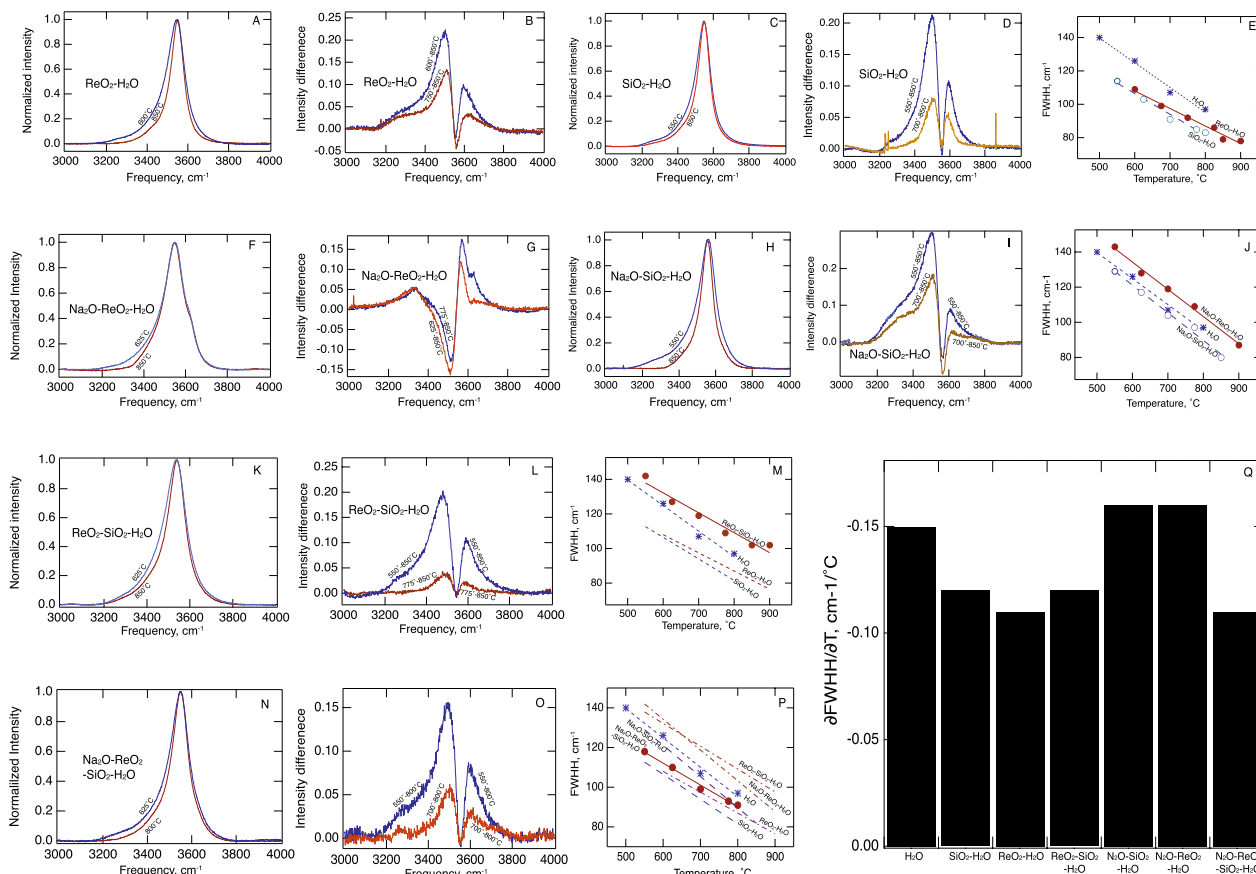
Fig. 8 Examples of Raman spectra in the high-frequency range (3000–4000 cm^{-1}) of fluids in all systems investigated at temperatures indicated on diagrams. Corresponding pressures can be read from Fig. 2. Spectra are normalized to the same acquisition time and slit width and then normalized to the maximum intensity within each spectrum. **A**, **C**, **F H**, **K**, and **N**. 3600 cm^{-1} envelope at temperature conditions indicated on each spectrum. Intensities are normalized to the highest intensity point in each spectrum. **B**, **D**, **G**, **I**, **L** and **O**. Difference spectra relative to the spectrum at the highest temperatures as indicated on each graph by temperature of each of the two spectra. Corresponding pressures can be read from Fig. 2. **E**, **J**, **M** and **P**. Full width at half height (FWHH) of the 3600 cm^{-1} envelopes from fluids in all systems as indicated on individual lines, as a function of temperature. Corresponding pressures can be read from Fig. 2. **Q** Comparison of temperature-dependence of FWHH from the high-frequency, ∂FWHH/∂T, spectra of all the fluids as indicated in the diagram

In high-frequency spectra of fluids equilibrated with $ReO_2 + SiO_2$ (ReO_2–SiO_2–H_2O) or $ReO_2 + SiO_2 + Na_2O$ (Na_2O–ReO_2–SiO_2–H_2O), the evolution of their $3600\ cm^{-1}$ envelopes is affected by the presence of SiO_2 (Fig. 8K, L, N, O). For example, for ReO_2–SiO_2–H_2O fluids, the temperature-dependent asymmetry on the low-frequency side of their $3600\ cm^{-1}$ Raman intensity envelope is less pronounced than in the $3600\ cm^{-1}$ envelope in spectra of fluids in the SiO_2-free ReO_2–H_2O system (Fig. 8A, B, D, G). Moreover, the $\partial FWHH/\partial T$ of the $3600\ cm^{-1}$ envelope in the ReO_2–SiO–H_2O and SiO_2–H_2O systems is essentially identical (Fig. 8Q). This similarity may reflect greater abundance of the SiO_2 components than the ReO_2 components in the ReO_2–SiO_2–H_2O fluid, so that the evolution of the FWHH with temperature is dominated by the width of intensity contributions from OH-groups in Si–OH bonds in both systems. It is unlikely that these effects could reflect hydrogen bonding because at the high temperatures of these experiments, hydrogen bonding cannot be detected in aqueous fluids (Foustoukos and Mysen 2012).

Addition of SiO_2 to the Na_2O–ReO_2–H_2O fluids results in $3600\ cm^{-1}$ envelopes resembling that of fluid in the ReO_2–SiO_2–H_2O system (Fig. 8K, N) more than the $3600\ cm^{-1}$ envelope in the NaO–ReO_2–H_2O spectra (Fig. 8F). This similarity can also be seen in the temperature-dependent FWHH, but this $\partial FWHH/\partial T$ differs significantly from the $\partial FWHH/\partial T$ of Na_2O–ReO–H_2O (Fig. 8Q). It is also notable that the temperature evolution of the $3600\ cm^{-1}$ from Na_2O–SiO_2–H_2O fluids is significantly different from that of the Na_2O–ReO_2–SiO_2–H_2O fluids (Figs. 8H, I, N, O, Q). This may be consistent with Si–OH bonding dominating in both the ReO–SiO_2–H_2O and Na_2O–ReO_2–SiO_2–H_2O fluids.

3.2 Species abundance in aqueous fluid
Integrated areas Raman bands from scattering of bonds in species dissolved in fluid, in principle can be transformed to species abundance. This can be done provided that a specified Raman intensity is calibrated against integrated intensity of Raman bands assigned to the same type of vibrations in spectra of a material with similar local structure and with known concentration of the type of bonding under consideration (Mysen 2015, 2018). However, in order for this method to yield reliable results, it is necessary that the optical absorption of the unknown and known materials does not differ.

This method has been applied successfully to abundance measurements of silicate species from Si–O vibrations in SiO_2-saturated aqueous fluids in equilibrium with quartz and TiO_2-saturated fluid in equilibrium with rutile (Mysen 2015, 2018). The method also has
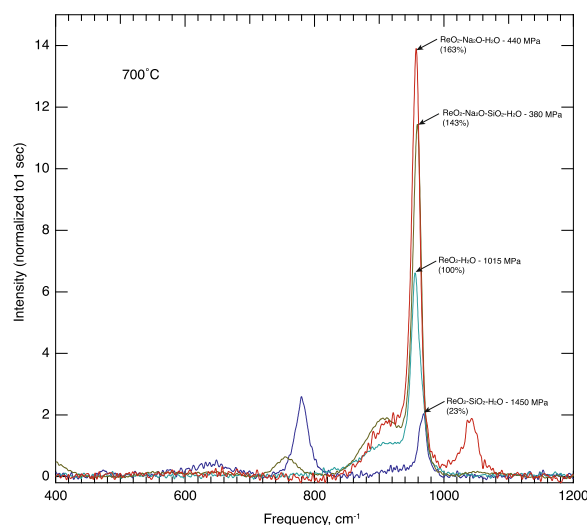

Fig. 9 Comparison of spectra recorded at 700 °C of Re-bearing fluids in low-frequency range. The spectrum from each system and corresponding pressure at 700 °C are indicated on each spectrum. Raman intensities are normalized to the same Raman setup parameters (acquisition time and slit width)

been used to report equilibria between structural units in silica-saturated H_2O at high temperature and pressure (Zotov and Keppler 2002; Mysen 2010). However, whenever the speciation changes or other local structural features surrounding a structural complex change, this method cannot be used.

In the present systems, a crystalline material to serve as calibrant for abundance in fluid could be ReO_2, for example. However, as seen in Fig. 1, the ReO_2 crystals are considerably darker than surrounding fluid. These crystals do, therefore, absorb a larger fraction of the incident laser light and a weaker Raman signal will be recorded from the sample than from a clear and colorless sample such as the surrounding aqueous fluids. Quantitative estimates of abundance of dissolved components in fluids in equilibrium with crystalline ReO_2, therefore, could not be carried out. As a result, only relative abundance variations from the fluid spectra will be discussed here.

An example of low-frequency Raman spectra from fluids in the four Re-bearing compositions recorded at 700 °C (but, therefore, at different pressures) illustrates how the overall composition of a system effects on the integrated intensity of Raman bands assigned to Re–O vibrations (Fig. 9), and, therefore, at least in principle, abundance of Re-components in fluids. Spectra recorded at different temperatures (and pressures) than those shown in Fig. 9 resemble those in Fig. 9.

For the $960\ cm^{-1}$ band, the intensity at 700 °C, which is proportional to the abundance of isolated ReO_4 complexes in fluid in most of the systems under study,
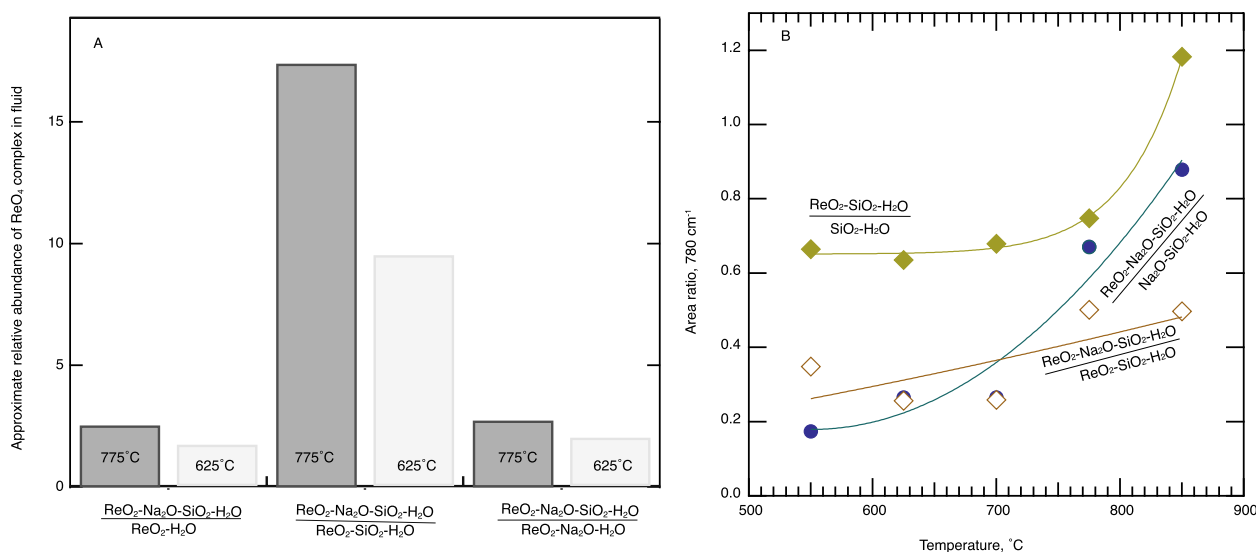
Fig. 10 **A** Relative abundance of isolated ReO$_4$ complexes in fluid expressed as ratio of systems and temperatures as indicated on diagram. The relative abundance is equal to the integrated intensity ratio of the 960 cm^{-1} Raman band (see text for discussion). The Raman bands are normalized to the same slit widths and acquisition times. Their ratio at the two different temperatures is not corrected for temperature-dependent Raman intensity (Long 1977). However, given the form of the temperature-dependence and the fact that it decreases to the fourth power with increasing Raman frequency (see Long 1977; Mysen et al. 1982b; for detailed discussion of these features), this assumption likely introduces a less than 10% error in individual intensities. Given that the same vibration in similar structural environments enters into this ration, this error likely cancels out. Relative abundance of isolated SiO$_4$ complexes in fluid expressed as ratio of systems and temperatures as indicated on diagram. The relative abundance is equal to the integrated intensity ratio of the 780 cm^{-1} Raman band assigned to Si–O stretch vibrations (see text for discussion). The Raman bands are normalized to the same slit widths and acquisition times

increases from that of the ReO$_2$–H$_2$O fluids (referenced as 100%) to as much as 163% for this band in the Raman spectrum of fluid in the Na$_2$O–ReO$_2$–H$_2$O system at the same temperature, but different pressure (Fig. 9). This intensity (and abundance) increase is 143% for the fluids in chemically more complex system, Na$_2$O–ReO$_2$–SiO$_2$–H$_2$O. It decreases to 23% for the ReO$_2$–SiO$_2$–H$_2$O system compared with the spectrum of ReO$_2$–H$_2$O system (Fig. 9).

The relative Re-species abundance differences illustrated in terms of different Raman intensity in the example in Fig. 9 very likely are near minimum values because the pressures in those 4 systems at 700 °C illustrated in this Figure are different and range from 380 to 1450 MPa for the Na$_2$O-bearing systems and from about 1000 to 1710 MPa for the data from fluids in systems without Na$_2$O (see exact pressures in Fig. 2 and also attached to each system designation for the 700°C spectra in Fig. 9).

Compared with alkali-free, but SiO$_2$-bearing systems, the ReO$_2$ solubility difference could differ by as much as a factor of 15–16 at temperatures near 800 °C compared to about a factor slightly less than 10 near 600–700 °C (Fig. 10). The solubility difference between the two Na$_2$O-bearing systems (Na$_2$O–ReO$_2$–SiO$_2$–H$_2$O and Na$_2$O–ReO$_2$–H$_2$O) is near 2 at the lowest temperatures to about 3 at the highest temperatures (Fig. 10).

Density of the aqueous fluids has been suggested to be a more appropriate means with which to compare solubility in the fluids in the various systems at temperatures and pressures because density is linked to both temperature and pressure (Kennedy 1950; Burnham et al. 1969; Wagner and Pruss 2002; Sanchez-Valle 2013) and because fluid density has been shown to be a variable that can be correlated oxide solubility in the fluid (Manning 1994; Pokrovski et al. 2005). For example, the rhenium solubility in fluid in the Na$_2$O–ReO$_2$–H$_2$O system can increase by 400–500% between 700 and 900 °C because pressure increases from 770 to 1075 MPa in this temperature range in this system. The H$_2$O density increases from ∼0.7 to ∼0.9 g/cm^3 (Burnham et al. 1969).

The intensity ratio changes of the 960 cm^{-1} band with temperature (and pressure) is consistent with the increased Re abundance as the density of aqueous fluid increases. It is also clear, for example, that for the systems where only isolated ReO$_4$ groups exist in the fluid (ReO$_2$–H$_2$O, ReO$_2$–SiO$_2$–H$_2$O, and Na$_2$O–ReO$_2$–SiO$_2$–H$_2$O), the relative rhenium concentration in fluid at constant fluid density increases by about an order of magnitude between ReO$_2$–SiO$_2$–H$_2$O and ReO$_2$–H$_2$O and by another approximately order of magnitude from ReO$_2$–H$_2$O fluids and Na$_2$O–ReO$_2$–SiO$_2$–H$_2$O fluids (Fig. 11). The data for the NaO–ReO$_2$–H$_2$O fluids differ because in
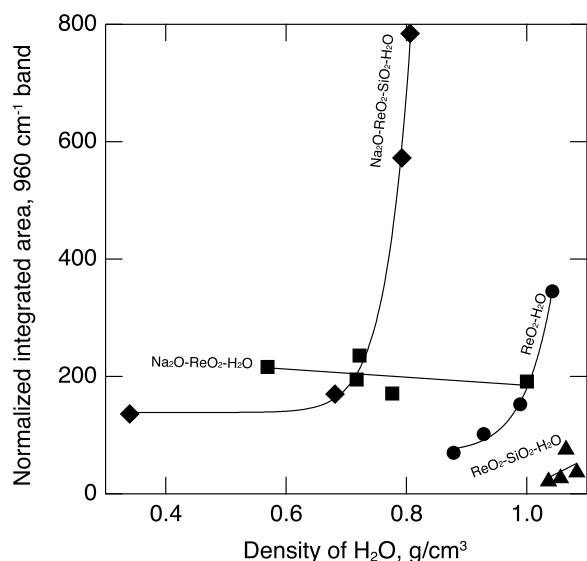
Fig. 11 Evolution of the intensity of the 960 cm^{-1} Raman band assigned to Re–O vibrations in ReO$_4$ complexes in the Re-bearing systems as a function of density of pure H$_2$O fluid. In all systems except Na$_2$O–ReO$_2$–H$_2$O, isolated ReO$_4$ complexes are the only Re-bearing complexes in the fluid. This means that for those systems, the integrated area, normalized to the same Raman spectroscopic setup, are proportional to the ReO$_4$ abundance, keeping in mind, nevertheless, that the temperature range for the data shown in the figure is between 600 and 900 °C. The highest temperatures also correspond to the greatest H$_2$O density because the pressure also increases with increasing temperature and the H$_2$O density is more sensitive to pressure than temperature in the temperature and pressure ranges of the experiments. As discussed in the caption to Fig. 9, absent correction for temperature, the proportionality of integrated area and ReO$_4$ abundance in the fluid might carry on the order of a 10% uncertainty. Density of H$_2$O was calculated with SUPCRT92 (Johnson et al. 1992), modified as described by Foustoukos and Mysen (2012) for expansion of pressures beyond the 500 MPa limit in the original SUPCRT92. The Raman bands are normalized to the same slit widths and acquisition times

this case some of the ReO$_2$ in the aqueous solution exists in more polymerized form than isolated ReO$_4$ tetrahedra. The integrated intensity of the 960 cm^{-1} band from those fluids is not, therefore, an appropriate expression of the ReO$_2$ solubility in the aqueous fluids.

In order to understand better the role of SiO$_2$ in the structural complexes of the solutes in the aqueous fluids, it is instructive to assess the differences in integrated areas of bands assigned to Si–O vibrations in fluids with and without ReO$_2$ in the system. As an example, the degree of polymerization of Si–O species in SiO$_2$-bearing, but ReO$_2$-free fluids generally is greater than when both ReO$_2$ and SiO$_2$ are present

such as Na$_2$O–SiO$_2$–H$_2$O compared with Na$_2$O–ReO$_2$–SiO$_2$–H$_2$O, for example. In the Na$_2$O–ReO$_2$–SiO$_2$–H$_2$O fluids, for all practical purposes there is evidence only for isolated OH-containing SiO$_4$ entities (the 780 cm^{-1} band in those spectra). Even in the latter case, the intensity ratio of the 780 cm^{-1} band [assigned to Si–O$^-$ stretch vibrations in Si(OH)$_4$ complexes] to that of the simpler ReO$_2$-free Na$_2$O–SiO$_2$–H$_2$O system is only about 0.2 as compared with about 0.6 for the intensity ratio of the 780 cm^{-1} band, ReO$_2$–SiO$_2$–H$_2$O/SiO$_2$–H$_2$O (Fig. 10B).

It follows from these observations that not only does Na$_2$O affect the structure and solubility of ReO$_2$ complexes in aqueous fluids, but SiO$_2$ also has an influence on those properties. In all systems, however, Si^{4+} and Re^{4+} in aqueous fluid remain in fourfold coordination with oxygen.

4 Conclusions

The Re solubility in aqueous fluids can vary by more than an order of magnitude in the temperature–pressure regime of the deep crust and upper mantle because of formation of complexes that also involves chemical interaction with other solutes. The solubility of such Re-bearing complexes is, in particular, dependent on the presence of alkali metals in the fluid. In this respect, the solubility behavior of rhenium in aqueous fluids resembles that of Ti^{4+} and Zr^{4+} (Antignano and Manning 2008; Hayden and Manning 2011; Wilke et al. 2012, 2013; Mysen 2012, 2015, 2022).

It is likely that the electronic properties of the metal cation in metal oxide-bearing fluids (i.e., alkali metals versus alkaline earth) could also affect Re solubility. In the case of SiO$_2$ solubility, for example, increasing electronegativity of the metal cation results in decreased silicate solubility at the same temperature and pressure such as when comparing the effects of Mg^{2+}, Ca^{2+}, and Na$^+$ on solubility of SiO$_2$, for example (Mysen et al. 2013; Mysen 2018).

Aqueous fluids from dehydrating slabs infiltrating overlying peridotite source can trigger partial melting in the peridotite wedge in subduction zones (Peacock 1993; Iwamori 1998; Schmidt and Poli 2014). It follows that the Re/Os budget in subduction zone peridotite affected by such fluids will depend on both the composition of the source of the fluid under which dehydration takes place. Such variations, in turn, can affect the Re-Os isotope systematics of source regions of magma in the Earth's upper mantle and, therefore, the Re-Os isotope systematics of magma itself.

Abbreviations

CCD　　　Charge-coupled detector
FWHH　　Full width at half height
HDAC　　Hydrothermal diamond anvil cell
HFSE　　High field strength element

Author contributions

As I am the sole author, I contributed 100% to the manuscript.

Availability of data and materials

All data are in the manuscript text and figures.

Declarations

Ethics approval and consent to participate

Not Applicable.

Consent for Publication

Not Applicable.

Competing interests

The author declares that he has no conflicts or competing interests.

References

Anderson GM, Burnham CW (1983) Feldspar solubility and the transport of aluminum under metamorphic conditions. Amer J Sci 283A:283–297

Antignano A, Manning CE (2008) Rutile solubility in H_2O, $H_2O–SiO_2$, and $H_2O–NaAlSi_3O_8$ fluids at 0.7–2.0 GPa and 700–1000 °C: Implications for mobility of nominally insoluble elements. Chem Geol 255(1):283–293. https://doi.org/10.1016/j.chemgeo.2008.07.001

Audétat A, Keppler H (2005) Solubility of rutile in subduction zone fluids, as determined by experiments in the hydrothermal diamond anvil cell. Earth Planet Sci Lett 232(3):393–402. https://doi.org/10.1016/j.epsl.2005.01.028

Azaroual M, Pascal ML, Roux J (1996) Corundum solubility and aluminum speciation in KOH aqueous solutions at 400 °C from 0.5 to 2.0 kbar. Geochim Cosmochim Acta 60(23):4601–4614. https://doi.org/10.1016/S0016-7037(96)00269-4

Bali E, Audetat A, Keppler H (2011) The mobility of U and Th in subduction zone fluids: an indicator of oxygen fugacity and fluid salinity. Contrib Mineral Petrol 161:597–613. https://doi.org/10.1007/s00410-010-0552-9

Bali E, Keppler H, Audetat A (2012) The mobility of W and Mo in subduction zone fluids and the Mo–W–Th–U systematics of island arc magmas. Earth Planet Sci Lett 351:195–207. https://doi.org/10.1016/j.epsl.2012.07.032

Bassett WA, Shen AH, Bucknum M, Chou IM (1994) A new diamond cell for hydrothermal studies to 2.5 GPa and from −190 to 1200 °C. Rev Sci Instr 64:2340–2345

Becker H (2000) Re–Os fractionation in eclogites and blueschists and the implications for recycling of oceanic crust into the mantle. Earth Planet Sci Lett 177(3):287–300. https://doi.org/10.1016/S0012-821X(00)00052-2

Becker KH, Cemič L, Langer KEOE (1983) Solubility of corundum in supercritical water. Geochim Cosmochim Acta 47(9):1573–1578. https://doi.org/10.1016/0016-7037(83)90183-7

Bernini D, Audetat A, Dolejs D, Keppler H (2013) Zircon solubility in aqueous fluids at high temperatures and pressures. Geochim Cosmochim Acta 119:178–187

Brawer SA, White WB (1975) Raman spectroscopic investigation of the structure of silicate glasses. I. The binary silicate glasses. J Chem Phys 63:2421–2432

Burnham CW, Holloway JR, Davis NF (1969) Thermodynamic properties of water to 1000 °C and 10,000 bars. Geol Soc America Special Paper 132:96p

Busey RH, Keller OL (1964) Structure of the aqueous pertechnetate ion by Raman and infrared spectroscopy. Raman and infrared spectra of crystalline $KTcO_4$, $KReO_4$, Na_2MoO_4, Na_2WO_4, $Na_2MoO_4·2H_2O$, and $Na_2WO_4·2H_2O$. J Chem Phys 41(1):215–225. https://doi.org/10.1063/1.1725625

Cody GD, Mysen BO, Lee SK (2005) Structure vs. composition: a solid state ^1H and ^{29}Si NMR study of quenched glasses along the $Na_2O–SiO_2–H_2O$ join. Geochim Cosmochim Acta 69:2373–2384

Crossley RJ, Evans KA, Evans NJ, Bragagni A, McDonald BJ, Reddy SM, Speelmanns IM (2020) Tracing Highly siderophile elements through subduction: insights from high-pressure serpentinites and 'hybrid' rocks from alpine Corsica. J Petrol. https://doi.org/10.1093/petrology/egaa030

D'Souza RJ, Canil D (2018) The partitioning of chalcophile elements between sediment melts and fluids at 3 GPa, 950–1050 °C with implications for slab fluids in subduction zones. Earth Planet Sci Lett 498:215–225

Diakonov I, Pokrovski G, Schott J, Castet S, Gout R (1996) An experimental and computational study of sodium-aluminum complexing in crustal fluids. Geochim Cosmochim Acta 60(2):197–211. https://doi.org/10.1016/0016-7037(95)00403-3

Foustoukos D, Mysen BO (2012) D/H isotope fractionation in the $H_2–H_2O$ system at supercritical water conditions: Compositional and hydrogen bonding effects. Geochim Cosmochim Acta 86:88–102

Frantz JD, Dubessy J, Mysen BO (1993) An optical cell for Raman spectroscopic studies of supercritical fluids and its application to the study of water to 500 °C and 2000 bar. Chem Geol 106:9–26

Furukawa T, Fox KE, White WB (1981) Raman spectroscopic investigation of the structure of silicate glasses. III. Raman intensities and structural units in sodium silicate glasses. J Chem Phys 153:3226–3237

Hanfland M, Syassen K, Fahy S, Louie SG, Cohen ML (1985) Pressure-dependence of the first-order Raman mode in diamond. Phys Rev B 31:6896–6899

Hayden LA, Manning CE (2011) Rutile solubility in supercritical $NaAlSi_3O_8–H_2O$ fluids. Chem Geol 284(1–2):74–81. https://doi.org/10.1016/j.chemgeo.2011.02.008

Hoffmann MM, Conradi MS (1997) Are there hydrogen bonds in supercritical water? J Am Chem Soc 119:3811–3817

Iwamori H (1998) Transportation of H_2O and melting in subduction zones. Earth Planet Sci Lett 160(1):65–80. https://doi.org/10.1016/S0012-821X(98)00080-6

Johnson JW, Oelkers EH, Helgeson HC (1992) SUPCRT92; a software package for calculating the standard molal thermodynamic properties of minerals, gases, aqueous species, and reactions from 1 to 5000 bar and 0 to 1000 °C. Comput Geosci 18(7):899–947

Kawamoto T, Ochiai S, Kagi H (2004) Changes in the structure of water deduced from the pressure dependence of the Raman OH frequency. J Chem Phys 120(13):5867–5870. https://doi.org/10.1063/1.1689639

Kennedy GC (1950) Pressure-volume-temperature relations in water at elevated temperatures and pressures. Am J Sci 248:540–564

Klein-BenDavid O, Pettke T, Kessel R (2011) Chromium mobility in hydrous fluids at upper mantle conditions. Lithos 125(1–2):122–130. https://doi.org/10.1016/j.lithos.2011.02.002

Lasaga AC (1982) Optimization of CNDO for molecular orbital calculation on silicates. Phys Chem Minerals 8:36–46

Le Losq CR, Moretti R, Neuville DR (2011) Water speciation in silicate melts investigated by Raman spectroscopy; implication for volcanic processes. Mineral Mag 75:1296

Le Losq C, Cody GD, Mysen BO (2015) Complex IR spectra of OH-groups in silicate glasses: implications for the use of the 4500 cm^{-1} IR peak as a marker of OH-groups concentration. Am Mineral 100:945–950. https://doi.org/10.2138/am-2015-5076

Liang Q, Meng YF, Yan CS, Krasnicki S, Lai J, Hemawan K, Shu H, Popov D, Yu T, Yang W, Mao HK, Hemley RJ (2013) Developments in synthesis, characterization, and application of large, high-quality CVD single crystal diamond. J Superhard Metr 35(4):195–213. https://doi.org/10.3103/s1063 457613040011

Long DA (1977) Raman spectroscopy. McGraw–Hill, New York

Louvel M, Sanchez-Valle C, Malfait WJ, Testemale D, Hazemann J-L (2013) Zr complexation in high pressure fluids and silicate melts and implications for the mobilization of HFSE in subduction zones. Geochim Cosmochim Acta 104:281–299. https://doi.org/10.1016/j.gca.2012.11.001

Manning CE (1994) The solubility of quartz in H_2O in the lower crust and upper mantle. Geochim Cosmochim Acta 58:4831–4840

Manning CE (2018) Fluids of the lower crust: deep is different. Ann Rev Earth Planet Sci 46:67–97

Mysen BO (2009) Solution mechanisms of silicate in aqueous fluid and H_2O in coexisting silicate melts determined in-situ at high pressure and high temperature. Geochim Cosmochim Acta 73(19):5748–5763. https://doi.org/10.1016/j.gca.2009.06.023

Mysen BO (2010) Speciation and mixing behavior of silica-saturated fluid at high temperature and pressure. Am Mineral 95:1807–1816

Mysen B (2012) High-pressure and high-temperature titanium solution mechanisms in silicate-saturated aqueous fluids and hydrous silicate melts. Am Mineral 97(7):1241–1251. https://doi.org/10.2138/am.2012.4084

Mysen B (2015) Hydrogen isotope fractionation and redox-controlled solution mechanisms in silicate-COH melt plus fluid systems. J Geophys Res Solid Earth 120(11):7440–7459. https://doi.org/10.1002/2015jb011954

Mysen B (2018) Silicate solution, cation properties, and mass transfer by aqueous fluid in the Earth's interior. Prog Earth Planet Sci 5(1):40. https://doi.org/10.1186/s40645-018-0198-1

Mysen B (2022) Fluids and physicochemical properties and processes in the Earth. Prog Earth Planet Sci 9(1):54. https://doi.org/10.1186/s40645-022-00516-0

Mysen BO, Virgo D (1986) Volatiles in silicate melts at high pressure and temperature. 1. Interaction between OH groups and Si^{4+}, Al^{3+}, Ca^{2+}, Na^+ and H^+. Chem Geol 57:303–331

Mysen BO, Yamashita S (2010) Speciation of reduced C–O–H volatiles in coexisting fluids and silicate melts determined in-situ to similar to 1.4 GPa and 800 °C. Geochim Cosmochim Acta 74(15):4577–4588. https://doi.org/10.1016/j.gca.2010.05.004

Mysen BO, Virgo D, Seifert FA (1982a) The structure of silicate melts: implications for chemical and physical properties of natural magma. Rev Geophys Space Phys 20:353–383

Mysen BO, Finger LW, Virgo D, Seifert FA (1982b) Curve-fitting of Raman spectra of silicate glasses. Am Mineral 67(7–8):686–695

Mysen BO, Mibe K, Chou IM, Bassett WA (2013) Structure and equilibria among silicate species in aqueous fluids in the upper mantle: experimental SiO_2–H_2O and MgO–SiO_2–H_2O data recorded in situ to 900 °C and 54 GPa. J Geophys Res Solid Earth 118(12):6076–6085. https://doi.org/10.1002/2013jb010537

Pascal ML, Anderson GM (1989) Speciation of Al, Si, and K in supercritical solutions: experimental study and interpretation. Geochim Cosmochim Acta 53:1843–1856

Peacock SM (1993) Large-scale hydration of the lithosphere above subducting slabs. Chem Geol 108(1):49–59. https://doi.org/10.1016/0009-2541(93)90317-C

Pokrovski GS, Roux J, Harrichoury J-C (2005) Fluid density control on vapor-liquid partitioning of metals in hydrothermal systems. Geology 33(8):657–660. https://doi.org/10.1130/g21475ar.1

Pokrovski GS, Borisova AY, Bychkov AY (2013) Speciation and transport of metals and metalloids in geological vapors. Rev Mineral Geochem 76(1):165–218. https://doi.org/10.2138/rmg.2013.76.6

Ragnarsdóttir KV, Walther JV (1985) Experimental determination of corundum solubilities in pure water between 400 and 700 °C and 1–3 kbar. Geochim Cosmochim Acta 49(10):2109–2115. https://doi.org/10.1016/0016-7037(85)90068-7

Sahle CJ, Sternemann C, Schmidt C, Lehtola S, Jahn S, Simonelli L, Huotari S, Hakala M, Pylkkanen T, Nyrow A, Mende K, Tolan M, Hamalainen K, Wilke M (2013) Microscopic structure of water at elevated pressures and temperatures. Proc Nat Acad Sci 110(16):6301–6306. https://doi.org/10.1073/pnas.1220301110

Sanchez-Valle C (2013) Structure and thermodynamics of subduction zone fluids from spectroscopic studies. Rev Mineral Geochem 76(1):265–309. https://doi.org/10.2138/rmg.2013.76.8

Schiferl D, Nicol M, Zaug JM, Sharma SK, Cooney TF, Wang S-Y, Anthony TR, Fleischer JF (1997) The diamond $^{13}C/^{12}C$ isotope Raman pressure sensor system for high temperature/pressure diamond-anvil cells with reactive samples. J Appl Phys 82:3256–3265

Schmidt MW, Poli S (2014) Devolatilization during subduction. In: Holland HD, Turekian KK (eds) Treatise on geochemistry, 2nd edn. Elsevier, Oxford, pp 669–701

Schmidt C, Seward TM (2017) Raman spectroscopic quantification of sulfur species in aqueous fluids: ratios of relative molar scattering factors of Raman bands of H_2S, HS^-, SO_2, HSO_4^-, SO_4^{2-}, $S_2O_3^{2-}$, S_3^- and H_2O at ambient conditions and information on changes with pressure and temperature. Chem Geol 467:64–75. https://doi.org/10.1016/j.chemgeo.2017.07.022

Seifert FA, Mysen BO, Virgo D (1982) Three-dimensional network structure in the systems SiO_2–$NaAlO_2$, SiO_2–$CaAl_2O_4$ and SiO_2–MgA_2O_4. Am Mineral 67:696–711

Stefánsson A, Driesner T, Bénézeth P (2013) Thermodynamics of geothermal fluids. Rev Mineral Geochem 76(1):1–4. https://doi.org/10.2138/rmg.2013.76.1

Sun W, Bennett VC, Eggins SM, Kamenetsky VS, Arculus RJ (2003) Enhanced mantle-to-crust rhenium transfer in undegassed arc magmas. Nature 422(6929):294–297. https://doi.org/10.1038/nature01482

Tassara S, González-Jiménez JM, Reich M, Saunders E, Luguet A, Morata D, Grégoire M, van Acken D, Schilling ME, Barra F, Nowell G, Corgne A (2018) Highly siderophile elements mobility in the subcontinental lithospheric mantle beneath southern Patagonia. Lithos 314–315:579–596. https://doi.org/10.1016/j.lithos.2018.06.022

Tropper P, Manning CE (2007) The solubility of corundum in H_2O at high pressure and temperature and its implications for Al mobility in the deep crust and upper mantle. Chem Geol 240(1–2):54–60. https://doi.org/10.1016/j.chemgeo.2007.01.012

Ulrich T, Mavrogenes J (2008) An experimental study of the solubility of molybdenum in H_2O and KCl–H_2O solutions from 500 to 800 °C and 150 to 300 MPa. Geochim Cosmochim Acta 72:2316–2330

Virgo D, Mysen BO, Kushiro I (1980) Anionic constitution of 1-atmosphere silicate melts: implications of the structure of igneous melts. Science 208:1371–1373

Wagner W, Pruss A (2002) The IAPWS formulation 1995 for the thermodynamic properties of ordinary water substance for general and scientific use. J Phys Chem Ref Data 31(2):387–535

Walrafen GE, Fisher MR, Hokmabadi MS, Yang WH (1986) Temperature-dependence of the low-frequency and high-frequency Raman-scattering from liquid water. J Chem Phys 85(12):6970–6982. https://doi.org/10.1063/1.451384

Walrafen GE, Hokmabadi MS, Yang WH, Piermarini GJ (1988) High-temperature high-pressure Raman-spectra from liquid water. J Chem Phys 92(15):4540–4542. https://doi.org/10.1021/j100326a056

Walrafen GE, Yang W–H, Chu YC (1999) Raman spectra from saturated water vapor to the supercritical fluid. J Phys Chem B 103:1332–1338

Watenphul A, Schmidt C, Jahn S (2014) Cr(III) solubility in aqueous fluids at high pressures and temperatures. Geochim Cosmochim Acta 126:212–227. https://doi.org/10.1016/j.gca.2013.10.054

Weinstock N, Schulze H, Müller A (1973) Assignment of v_2 (E) and v_4 (F2) of tetrahedral species by the calculation of the relative Raman intensities: The vibrational spectra of VO_4^{3-}, CrO_4^{2-}, MoO_4^{2-}, WO_4^{2-}, MnO_4^-, TcO_4^-, ReO_4^-, RuO_4, and OsO_4. J Chem Phys 59(9):5063–5067. https://doi.org/10.1063/1.1680724

Wilke M, Schmidt C, Dubrail J, Appel K, Borchert M, Kvashnina K, Manning CE (2012) Zircon solubility and zircon complexation in H_2O+Na_2O+SiO_2 ± Al_2O_3 fluids at high pressure and temperature. Earth Planet Sci Lett 349–350:15–25

Wilke M, Schmidt C, Dubrail J, Appel K, Borchert M, Kvashnina K, Manning CE (2013) Zircon solubility and zirconium complexation in H_2O+Na_2O+SiO_2

± Al_2O_3 fluids at high pressure and temperature. Earth Planet Sci Lett 373:242–243. https://doi.org/10.1016/j.epsl.2013.04.010

Wohlers A, Manning CE, Thompson AB (2011) Experimental investigation of the solubility of albite and jadeite in H_2O, with paragonite plus quartz at 500 and 600 °C, and 1–2.25 GPa. Geochim Cosmochim Acta 75(10):2924–2939. https://doi.org/10.1016/j.gca.2011.02.028

Zotov N, Keppler H (2000) In-situ Raman spectra of dissolved silica species in aqueous fluid to 900 °C and 14 kbar. Am Mineral 85:600–603

Zotov N, Keppler H (2002) Silica speciation in aqueous fluids at high pressures and high temperatures. Chem Geol 184:71–82

Publisher's Note